Safe Coordination of Human-Robot Firefighting Teams

Anonymous Authors

Anonymous Affiliation, Anonymous University
anonymous.email@anonymous.author

Abstract

Wildfires are destructive and inflict massive, irreversible harm to people's lives and natural resources. Researchers have proposed employing unmanned aerial vehicles (UAVs) to provide firefighters with real-time tracking information. Yet, these approaches do not reason about fire's track, including current fire location, measurement, and uncertainty, and propagation. We propose a model-predictive, probabilistically-safe, distributed control algorithm for human-robot collaboration in wildfire fighting. The proposed algorithm overcomes the limitations of prior work by explicitly estimating the latent fire propagation dynamics to enable intelligent, time-extended coordination of the UAVs in support of on-the-ground, human firefighters. We derive a novel, analytical bound that enables UAVs to distribute their resources to provide a probabilistic guarantee of the humans' safety preserving the ability to cover the entire fire.

1 Introduction

Wildfires are notorious for their destructive ability to inflict massive, irreversible damages to both people's lives and natural resources. According to the Insurance Information Institute [Institute, 2018] more than 122,000 wildfires burned more than 24 million acres, killed more than 12,000 people and caused about twenty billion dollars of damage during 2016-2018 within the United States.

Fighting wildfires is a dangerous task and requires accurate online information regarding firefront location, size and scale, shape and the propagation velocity [Martinez-de Dios *et al.*, 2008; Stipaniev *et al.*, 2010; Sujit *et al.*, 2007]. Historically, researchers have sought to extract images from overhead satellite feeds to estimate fire location information [Fujiwara and Kudoh, 2002; Kudoh and Hosoi, 2003; Casbeer *et al.*, 2006]. However, the resolution of satellite images is typically too low to do more than simply detect the existence of fire [Casbeer *et al.*, 2006]. Firefighters need frequent high quality images (i.e. information update) to monitor the fire propagation and choose the most effective fighting policy accordingly and even more importantly, stay safe.
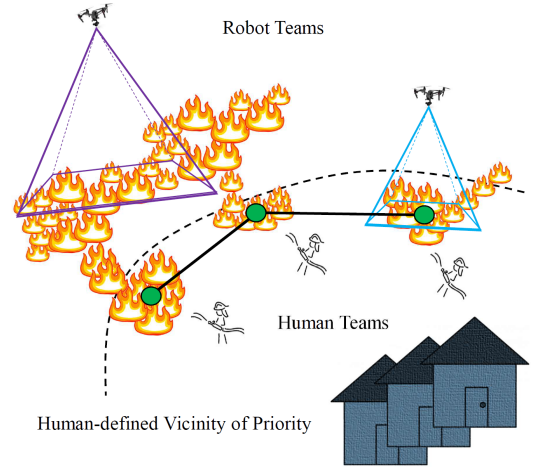

Figure 1: This figure depicts the proposed safe coordination of human-robot firefighting teams.

Recent advances in UAV technology have opened up the possibility of providing real-time, high-quality fire information to firefighters. However, the control of UAVs in this setting provides particular challenges. Effective cooperation normally requires that all individual UAVs have a comprehensive knowledge regarding the state of every other team member in order to coordinate their actions. This assumption is not always appropriate due to communication constraints and complexities. Accordingly, researchers typically seek to develop distributed coordination algorithms that reduce the need for explicit communication [Beard *et al.*, 2006; McIntire *et al.*, 2016; Nunes and Gini, 2015; Choi *et al.*, 2009].

Previous approaches to distributed control of UAVs have typically sought to maximize the "coverage" of the fire. In the works of Schwager *et al.* [2011] and, more recently Pham *et al.* [2017], coverage is the average pixel-density across the entire fire. However, these approaches do not explicitly reason (i.e., through tracking and filtering) about the fire state (i.e., position, velocity, and associated uncertainty) nor do they attempt to develop a predictive model for fire propagation by key parameters, e.g., fire spread-rate due to available fuel and vegetation. Furthermore, the location of the firefront is typically modelled as the "coolest" part of the fire visible

via infrared sensors; however, this is not always accurate Pastor et al. [2003].

In this paper, we overcome key limitations in prior work by developing an algorithmic framework to provide a model-predictive mechanism that enables firefighters on the ground to have probabilistic guarantees about their time-varying proximity to the fire. In our approach, we explicitly estimate the latent fire propagation dynamics via a multi-step Adaptive Extended Kalman Filter (AEKF) predictor and the simplified FARSITE wildfire propagation mathematical model [Finney, 1998]. This model enables us to develop straightforward distributed control adapted from vehicle routing literature [Cho and Choi, 2019; Laporte, 1992; Toth and Vigo, 2002; Golden et al., 1980] to enable track-based fire coverage.

In addition to this coverage controller, we derive a set of novel, analytical bounds that enable UAVs to enable probabilistic-safe coordination of the UAVs in support of on-the-ground, human firefighters. We investigate three different wildfire scenarios where (1) wildfire is almost stationary, (2) wildfire moves but does not grow (e.g. spawn) considerably and (3) wildfire moves quickly and multiplies. We derive analytic safe-to-work, probabilistic, temporal upper-bounds for each case to give firefighters the ability to understand how long they have until they must evacuate a location. We empirically evaluate our approach against simulated wildfires alongside contemporary approaches for UAV coverage [Pham et al., 2017] as well as against reinforcement learning techniques, demonstrating the promising utility of our approach.

2 Preliminaries

In this Section, we first introduce the simplified FARSITE wildfire propagation mathematical model and calculate the fire dynamics. We then review the fundamentals of AEKF.

2.1 FARSITE: Wildfire Propagation Dynamics

Fire Area Simulator (FARSITE) wildfire propagation mathematical model was first introduced by Finney [1998] which is now widely used by the USDI National Park Service, USDA Forest Service, and other federal and state land management agencies. The model has been employed to simulate a wildfire's spread, accounting for heterogeneous conditions of terrain, fuels, and weather and their influence on fire dynamics. The full FARSITE model includes complex equations for firefront location updates, and precise model implementation requires a significant amount of geographical, topographical and physical information on terrain, fuels and weather. Moreover, the precise implementation of the FARSITE model is highly computationally expensive and thus, researchers tend to modify the model by considering several simplifying assumptions Pham et al. [2017]. The wildfire propagation dynamics using a simplified FARSITE model can be stated as shown in Equations 1 and 2.

$$q_t^i = q_{t-1}^i + \dot{q}_{t-1}^i \delta t \tag{1}$$

$$\dot{q}_t^i = \frac{d}{dt}\left(q_t^i\right) \tag{2}$$

In Equations 1 and 2, q_t^i indicates the location of firefront i at time t and $\dot{q}_t^i$ is its growth rate (i.e. fire propagation velocity) and is a function of fire spread-rate (R_t, e.g. fuel and

vegetation coefficient), wind speed (U_t) and wind azimuth (θ_t) which are available to our system through weather forecasting equipment at each time t.

2.2 Adaptive Extended Kalman Filter (AEKF)

The Kalman Filter is an optimal estimation method for linear systems with additive independent white noise in both transition and observation systems [Kalman and others, 1960; Kalman and Bucy, 1961; Kalman, 1960]. For nonlinear systems, an Extended Kalman Filter (EKF), which adapts multivariate Taylor series expansion techniques to locally linearize functions, can be leveraged. In an EKF, the state transition and observation models need not be linear but may instead be functions that are differentiable and therefore linearizeable, as shown in Equations 3 and 4, where $f(s_{t-1}, u_t)$ and $h(s_t)$ are the state transition and observation models respectively, connecting states s_t and s_{t-1} at $t-1$ and t.

$$s_t = f(s_{t-1}, u_t) + \omega_t \tag{3}$$

$$z_t = h(s_t) + \nu_t \tag{4}$$

Taking u_t as control input, function f computes the predicted state at time t from the previous estimate at time $t-1$ where h maps the predicted state estimate to predicted state observation. Variables ω_t and ν_t model the process and observation noises, respectively, and are assumed to be zero mean multivariate Gaussian noise with covariances Q_t and R_t.

AEKF: Prediction Step

The first step in EKF is the prediction step during which a prediction of the next to-be-observed state is estimated. The predicted state estimate is measured using Equation 5 and the predicted covariance estimate can be calculated shown in Equation 6, where F_t is the state transition matrix and defined in Equation 7 as the Jacobian of the fire propagation model (Equation 7).

$$\hat{s}_{t|t-1} = f(\hat{s}_{t-1|t-1}, u_t) \tag{5}$$

$$P_{t|t-1} = F_t P_{t-1|t-1} F_t^T + Q_t \tag{6}$$

$$F_t = \left.\frac{\partial f}{\partial s}\right|_{\hat{s}_{t-1|t-1}, u_t} \tag{7}$$

$$\hat{s}_{t+r|t} = F_t^{r-1} s_{t|t-1} \tag{8}$$

It can be shown that a multi-step prediction of the state from r steps ahead $\hat{s}_{t+r|t}$ can be obtained given the measurements and observations at time t [Taragna, 2011] as shown in Equation 8.

AEKF: Update Step

The state and covariance estimates are updated in this step as shown in Equations 9-10, where $K_t = P_{t|t-1} H_t^T S_t^{-1}$ is the near-optimal Kalman gain and $\tilde{y}_t = z_t - h(\hat{s}_{t|t-1})$ is the measurement residual. Moreover, S_t is the covariance residual and can be measured as shown in Equation 11, where H_t is the observation Jacobian matrix calculated as shown in Equation 12. As in Equation 8, the measurement residual of the observation model $h(s_t)$ at r steps into the future can be

obtained through Equation 13.

$$\hat{s}_{t|t} = \hat{s}_{t|t-1} + K_t \tilde{y}_t \tag{9}$$

$$P_{t|t} = (I - K_t H_t) P_{t|t-1} \tag{10}$$

$$S_t = H_t P_{t|t-1} H_t^T + R_t \tag{11}$$

$$H_t = \left. \frac{\partial h}{\partial s} \right|_{\hat{s}_{t|t-1}} \tag{12}$$

$$S_{t+r|t} = H_t F_t^{r-1} P_{t|t-1} \left(H_t F_t^{r-1} \right)^T + R_t \tag{13}$$

We leverage the adaptive extended Kalman filter [Akhlaghi *et al.*, 2017], which introduces innovation and residual based updates for process and observation noise covariances as shown in Equations 14-15. These updates remove the assumption of constant covariances Q_t and R_t.

$$Q_t = \alpha Q_{t-1} + (1 - \alpha) \left(K_t d_t d_t^T K_t^T \right) \tag{14}$$

$$R_t = \alpha R_{t-1} + (1 - \alpha) \left(\tilde{y}_t \tilde{y}_t^T + H_t P_{t|t-1} H_t^T \right) \tag{15}$$

Q_t and R_t are adaptively estimated as the Kalman filter leverages its observations to improve the predicted covariance matrix $P_{t|t-1}$ by applying Equations 14-15. This AEKF's multi-step prediction and error propagation provide the capability to derive an anlytical condition for the safety of human firefighters, as we will see in Section 3.2. To the authors' knowledge, this has not yet been explored in the related literature.

3 Method

The proposed algorithm for safe human-robot coordination in wildfire fighting can be summarized as follows: Initially, all available drone resources are distributed to cover the wildfire by generating a search graph and clustering the hotspots to generate an optimal path for each drone. Hotspots can be detected through vision or thermal cameras [Merino *et al.*, 2010; Yuan *et al.*, 2015]. We assume that firefighters' locations are known to the system through common locating devices such as GPS. Upon receiving a support request from a human team, one of the drones conducts a "feasibility test" based on an analytical, probabilistic bound we derive in Section 3.1 Equations 17, 18, and 21, to determine whether the UAV can safely protect the human firefighters. This bound determines an upper bound on the time, T_{UB}, required to cover each fire in the vicinity of the human firefighters. T_{UB} is compared to the maximum time allowable for each firetrack to propagate before measurement – derived from the AEKF model – so that the residual post-measurement is less than the residual after the last time a given firefront location was observed. This test is presented in Section 3.2 with Equation 23. If the test is satisfied, a near-optimal tour is computed via a k-opt procedure. If the test fails, the UAV recruits more UAVs to assist until this bound is satisfied, divvying up the responsibilities for covering the fire locations. Next, we describe in detail each component of our overall method.

The proposed framework depends on the calculated upper bound traverse time, T_{UB}, which depends on the propagation velocity and growth rate of the wildfire. Details of different wildfire scenarios and the analytical traverse time upper bound for each case are presented in the following section.
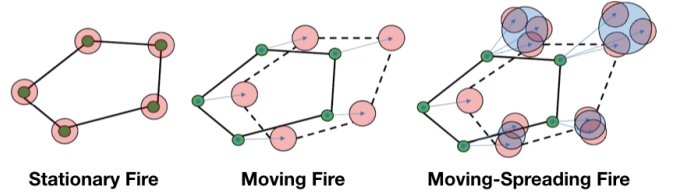

Figure 2: This figure depicts the three wildfire scenarios we consider: Case 1: near-stationary (Left), Case 2: wildfire moves but does not grow considerably (Center), and Case 3: wildfire moves quickly and multiplies (Right). The green dots and red circles represent current and next-step locations of firefronts and the blue circles indicate the Steiner zones.

3.1 Probabilistic Safety for Coordination

In this section we develop a probabilistic upper bound, T_{UB} on the time required by a drone to service each fire location (i.e., observe once). This upper bound is then used in Section 3.2, Equation 23 to determine whether a drone can be probabilistically guaranteed to service each fire location fast enough to ensure a bounded track residual for each fire. We derive three bounds, one for each of the following fire scenarios: the (1) wildfire is almost stationary, (2) wildfire moves but does not grow (e.g. spawn) considerably and (3) wildfire moves quickly and multiplies. Figure 2 depicts these scenarios.

For the derivation, we reason about the velocity of the fire at the α confidence level, i.e., the probability the velocity is greater is $1 - \alpha$. We set $\alpha = 0.05$ for our experiments. Further, we assume each fire's velocity is conditionally independent given the latent fire dynamics, which we estimate explicitly in our AEKF model. As such, the probability that our bounds are correct is given by Equation 16, where T^* is the actual maximum time the drone can go without visiting any $q \in Q$ and T_{UB} is our bound. [1]

$$Pr[T_{UB} \geq T^*] \leq 1 - \prod_{q \in Q} 1 - \alpha \tag{16}$$

Case 1: Stationary Fire

The first wildfire scenario is when the fire is almost stationary. Considering a search graph made of all hotspots to visit as vertices and paths to traverse as edges, a minimum spanning tree (MST) can be calculated quickly as the initial path. Note that the MST path (e.g. the Hamiltonian Cycle computed from the MST) is not the fastest possible path, but it is fast to generate. Therefore, drones utilize the k-opt algorithm to iteratively improve the path and bring it closer to optimal. This process ensures a quick, sound way to guarantee safety for the people on the ground. Once a consensus is reached with respect to the safety of human firefighters, UAVs can spend time making the actual tours more efficient. We derive the upper bound time to complete a tour to all firefront locations as the Hamiltonian path of the MST path (denoted with

---

[1]A formal proof and derivations is included in our supplementary version, available at https://github.com/firefront-tracking/Safe-Coordination-of-Human-Robot-Firefighting-Teams

temporal cost MST) for a drone with velocity v in Equation 17.

$$T_{UB}^{(C1)} = \frac{2MST}{v} \qquad (17)$$

Case 2: Moving Fire
The second scenario to consider is a fire that moves but does not grow (e.g. spawn) considerably. In this case, the number of nodes $|Q|$ (e.g. discretized firefront points) and the velocity of the propagating fire need to be taken into account. Our upper bound on the time a UAV has to revisit each fire location is given by Equation 18, where $\widehat{q_t^\xi}\big|_\alpha$ is the estimated speed of fire q in the $\xi \in x, y$ direction evaluated at confidence interval defined by α.

$$T_{UB}^{(C2)} = \frac{MST}{\frac{v_m}{2} - 2\zeta^\alpha\left(|Q| - 1\right)} \qquad (18)$$

$$\zeta^\alpha = \arg\max_{q,q'} \sqrt{\left(\widehat{q_t^x}\big|_\alpha\right)^2 + \left(\widehat{q'_t^y}\big|_\alpha\right)^2} \qquad (19)$$

In Equation 18, we assume a worst-case speed for all fires propagating at a rate of the speed of the the fire with the fastest speed in the x-direction and the fire with the fastest speed in the y-direction, as shown in Equation 19. By setting α, we can control the degree of confidence in our system at the cost of making the UAV coordination problem more difficult. This independence assumption and uniformity of fastest and universal speed is a worst-case assumption.

To arrive at this bound, we begin by considering the cost of traveling to each fire under the stationary case, $T_{UB}^{(C1)}$. If the fire locations are moving, the edges of the Hamiltonian cycle connected each fire location will shrink or expand. In the worst case, we can assume that each edge expands according to two times the velocity of the fastest fire location. Considering that the drone has $|Q|$ fires to consider, this yields $(|Q| - 1)$ edges that may expand in the MST, with two times that quantity accounting for the Hamiltonian path. We note that the total expansion is a function of the time the fire is allowed to expand, which is a self-referencing equation, as shown in Equation 20. However, we can easily solve for $T_{UB}^{(C2)}$ to arrive at Equation 18.

$$T_{UB}^{(C2)} = T_{UB}^{(C1)} + 2 * (|Q| - 1)\, \zeta^\alpha * T_{UB}^{(C2)} \qquad (20)$$

Case 3: Moving-Spreading Fire
The third scenario we consider is a wildfire that moves and grows quickly. Single nodes of fire expand over time and escape the drone's field of view (FOV). The drones need to consider the time that it takes for a spawning point q to escape their FOV, given its velocity and the width of the FOV g. The upper bound for traversal time allowed to maintain the track quality of each fire is shown in Equation 21, where $\gamma = \frac{4|Q|(\zeta^\alpha)^2}{gv}$, $\beta = 1 + \frac{2|Q|\zeta^\alpha}{v}$, and $\delta = \frac{MST}{\frac{v}{2} - 2\zeta^\alpha(|Q|-1)}$.

$$T_{UB}^{(C3)} = \frac{-\beta + \sqrt{\beta^2 - 4\gamma\delta}}{2\gamma} \qquad (21)$$

The width of the FOV for a drone d with altitude p_d^z is the half-angle θ of the camera as $g = 2p_d^z \tan\theta$.

To arrive at this bound, we begin by considering the time to traverse to each, moving firefront, and the time to cover the area possibly engulfed by the growth of each firefront, as shown in Equation 22. The first term of this equation brings $T_{UB}^{(C2)}$ from Equation 18. However, we must also account for the fact that the fires are allowed to spread for $T_{UB}^{(C3)}$ units of time instead of only $T_{UB}^{(C2)}$. Second, we must consider how much growth a fire location will experience. For a specific fire, q, the fire will grow no more than $2\,\widehat{q_t^x}\big|_\alpha T_{UB}^{(C3)}$ along the x-direction and no more than $2\,\widehat{q_t^y}\big|_\alpha T_{UB}^{(C3)}$ along the y-direction at the α confidence level. If we assume a vertical scanning pattern, the total number of passes the drone would take from left to right is given by $\lceil 2\,\widehat{q_t^x}\big|_\alpha T_{UB}^{(C3)}/g \rceil$, and the total distance traversed for each pass is $2\,\widehat{q_t^y}\big|_\alpha T_{UB}^{(C3)}$.

$$T_{UB}^{(C3)} = T_{UB}^{(C2)}\Big|_{C3} + \sum_q \frac{2}{v}\,\widehat{q_t^y}\Big|_\alpha T_{UB} \left\lceil \frac{2\,\widehat{q_t^x}\big|_\alpha T_{UB}^{(C3)}}{g} \right\rceil \qquad (22)$$

We make the following two, conservative, simplifying assumptions: First, we remove the ceiling operator and add one to the term inside the operator to achieve continuity. Second, we adopt a similar approach to Case 2 by assuming the area required to cover to account for the growth of each fire location is upper-bounded by $|Q|$ times the area of growth for a hypothetical fire growing quickest. With these two conservative, simplifying assumptions, we can easily arrive at the bound in Equation 22.[2]

3.2 Human Safety Module

Close-enough Traveling Salesman Problem
The first step in our human safety module is to generate a search graph with firefront points within human vicinity as the vertices and distances in-between as the edges. For this purpose, we leverage the close-enough traveling salesman problem (CE-TSP) with Steiner zone Wang *et al.* [2019] variable neighborhood search. In CE-TSP the agent does not need to visit the exact locations of each fire. Instead, the agent only gets "close enough" to each goal.

In the application of monitoring firefront hotspots, a UAV can observe multiple nodes within its FOV and thus, does not need to travel to the exact locations of each firefront point. Instead, we first identify the overlapping disks between k fire points as their corresponding Steiner zone Wang *et al.* [2019] and choose a node from the identified Steiner areas in order to be a new vertex in our tour instead of the corresponding k points. Second, we construct a quick feasible MST tour that passes through all Steiner zones and single fire points. Finally, we iteratively improve the constructed path through k-opt algorithm to increase the service speed. Note that as mentioned before, the last step will take place after the probabilistic human safety condition (e.g. URR) is satisfied.

---

[2]See Appendix

Analytical Safety Condition: Uncertainty Residual Ratio
Upon reaching to a new node within the human vicinity, the UAV calculates two quantities (1) the time required to complete a tour generated in the previous step using the analytical time upper bound Equations T_{UB} and (2) the current measurement residual covariance through Equation 11. Leveraging these two parameters, now Equation 13 can be used to predict an estimation of the residual T_{UB} steps into the future. We introduce the uncertainty residual ratio (URR) as shown in Equation 23.

$$URR_t^q = \frac{S_{t+T_{UB}|t}}{S_{t|t-1}} \leq 1, \forall q \in Q \tag{23}$$

The URR_t^q is an indicator of the scale to which the UAV is capable of tracking the fire point q within the vicinity of the humans, without losing tracking information. A URR greater than one demonstrates a quickly growing or propagating wildfire towards the human team , about which the UAV will not be capable of providing online information while completing a tour before the situation becomes dangerous and retreat is necessary. Similarly, a URR smaller than 1 indicates that online information can be provided while keeping track of the fire and ensuring the safety of humans.

If the URR condition is not satisfied for a node, the generated path in the CE-TSP step is partitioned into two paths and another UAV is recruited from the available resources. This process is repeated until URR_t^q is satisfied for all q and t. In order to calculate the residuals and in the URR Equation in 23, we use the adaptive extended Kalman filter (AEKF). The process and observation models derivations of AEKF are detailed in the following sections.

3.3 Uncertainty and Residual Prediction

For the purpose of measurement residual estimation, we use EKF to predict a distribution and accordingly a measurement covariance for each firefront point through linear error propagation techniques. Considering q_{t-1} as the location of firefronts at current time and p_{t-1} as the UAV coordinates, desired is a prediction of firefront location $\hat{q}_t$ one step forward in time, given the current firefront distribution (q_{t-1}), fire propagation model with current parameters ($\mathcal{M}_{t-1}$) and UAV observation model of the field ($\mathcal{O}_{t-1}$). In other words, $\hat{q}_t = \arg\max_{q_t} \rho\left(q_{t-1}, p_{t-1}, \mathcal{M}_{t-1}, \mathcal{O}_{t-1}, q_t\right)$.

We now compute the terms from the EKF equations presented in Section 2.2, where wildfire propagation model $\mathcal{M}$ and drones observation model $\mathcal{O}$ are functions f and h in Equation 3-4. Using the aforementioned notations, the EKF state transition and observation Equations can now be stated in Equations 24 and 25, where $p_{t-1} = [p_t^x, p_t^y, p_t^z]$ is the physical location of UAV.

$$q_t = f_{t-1}\left(q_{t-1}, p_{t-1}, R_{t-1}, U_{t-1}, \theta_{t-1}\right) + \omega_t \tag{24}$$
$$\hat{q}_t = h_t\left(q_t, p_{t-1}\right) + \nu_t \tag{25}$$

We reform the state transition equation in 24 to account for all associating parameters given by $\mathcal{S}_t = \left[q_t^x, q_t^y, p_t^x, p_t^y, p_t^z, R_t, U_t, \theta_t\right]^T$. Furthermore, $\Phi_t = \left[q_t^x, q_t^y, p_t^x, p_t^y, p_t^z, R_t, U_t, \theta_t\right]^T$ is a mapping vector through which the predicted fire dynamics and drones

locations are translated into a unified angle-parameter vector $\hat{\Phi}_t = \left[\varphi_t^x, \varphi_t^y, \hat{R}_t, \hat{U}_t, \hat{\theta}_t\right]^T$. The angle-parameters (i.e. φ_t^x and φ_t^y) contains information regarding both firefront location $[q_t^x, q_t^y]$ and UAV coordinates $[p_t^x, p_t^y]$. By projecting the looking vector of UAV to planar coordinates, the angle parameters are calculated as $\varphi_t^x = \tan^{-1}\left(\frac{q_t^x - p_t^x}{p_t^z}\right)$ and $\varphi_t^y = \tan^{-1}\left(\frac{q_t^y - p_t^y}{p_t^z}\right)$.

The next step is to calculate the state transition Jacobian matrices F_t and H_t in Equations 7 and 27, respectively [3], where $t' = t - 1$ and superscript (3) represents number of column and row repetition for all $[p_t^x, p_t^y, p_t^z]$.

$$\left.\frac{\partial f}{\partial \mathcal{S}_i}\right|_{\hat{\Phi}_{t'}} = \begin{array}{c} \\ q_t^x \\ q_t^y \\ p_t^{(3)} \\ R_t \\ U_t \\ \theta_t \end{array} \begin{pmatrix} q_{t'}^x & q_{t'}^y & p_{t'}^{(3)} & R_{t'} & U_{t'} & \theta_{t'} \\ 1 & 0 & 0^{(3)} & \frac{\partial q_t^x}{\partial R_{t'}} & \frac{\partial q_t^x}{\partial U_{t'}} & \frac{\partial q_t^x}{\partial \theta_{t'}} \\ 0 & 1 & 0^{(3)} & \frac{\partial q_t^y}{\partial R_{t'}} & \frac{\partial q_t^y}{\partial U_{t'}} & \frac{\partial q_t^y}{\partial \theta_{t'}} \\ 0 & 0 & 0^{(3)} & 0 & 0 & 0 \\ 0 & 0 & 0^{(3)} & 1 & 0 & 0 \\ 0 & 0 & 0^{(3)} & 0 & 1 & 0 \\ 0 & 0 & 0^{(3)} & 0 & 0 & 1 \end{pmatrix} \tag{26}$$

$$\left.\frac{\partial h}{\partial \Phi_i}\right|_{\hat{\Phi}_{t|t-1}} =$$

$$\begin{array}{c} \\ \varphi_t^x \\ \varphi_t^x \\ \hat{R}_t \\ \hat{U}_t \\ \hat{\theta}_t \end{array} \begin{pmatrix} q_t^x & q_t^y & p_t^x & p_t^y & p_t^z & R_t & U_t & \theta_t \\ \frac{\partial \varphi_t^x}{\partial q_t^x} & 0 & \frac{\partial \varphi_t^x}{\partial p_t^x} & 0 & \frac{\partial \varphi_t^x}{\partial p_t^z} & 0 & 0 & 0 \\ 0 & \frac{\partial \varphi_t^y}{\partial q_t^y} & 0 & \frac{\partial \varphi_t^y}{\partial p_t^y} & \frac{\partial \varphi_t^y}{\partial p_t^z} & 0 & 0 & 0 \\ 0 & 0 & 0 & 0 & 0 & 1 & 0 & 0 \\ 0 & 0 & 0 & 0 & 0 & 0 & 1 & 0 \\ 0 & 0 & 0 & 0 & 0 & 0 & 0 & 1 \end{pmatrix} \tag{27}$$

3.4 Distributed Coverage

While UAVs are not required to monitor the firefronts directly and provide human firefighters with safety information, they will explore the rest of the wildfire. A discussed earlier, distributed exploration and coverage is more efficient and practical as states of agents are hardly known to other agents due to communication constraints. In this section we propose a distributed framework similar to our human safety module. The steps to our distributed coverage module are as follows: after detecting the fire-map and hotspots through visual or thermal cameras, a set of fire points based on the aforementioned Steiner zone variable neighborhood search method are generated. The set of nodes are partitioned (e.g. K-means clustering) according to the number of available UAVs. Each drone is assigned to one partition by solving a simple constraint satisfaction problem (CSP) with drones as variables, partitions as domains, and distance to the center of the partition as the constraints. Afterwards, an optimal path for coverage and tracking is found through k-opt algorithm. The upper bound time, T_{UB}, is then calculated for a fire point in the center of the drone's FOV. T_{UB} provides the drone with an estimate of how long it will take the fire to escape its FOV, based on fire propagation velocity. When a route is found, based on the velocity of the fire, UAVs can use it for the next T_{UB} timesteps

---

[3]See Appendix

(a) Drones required for human safety   (b) Fire-map uncertainty   (c) Comparison to prior work
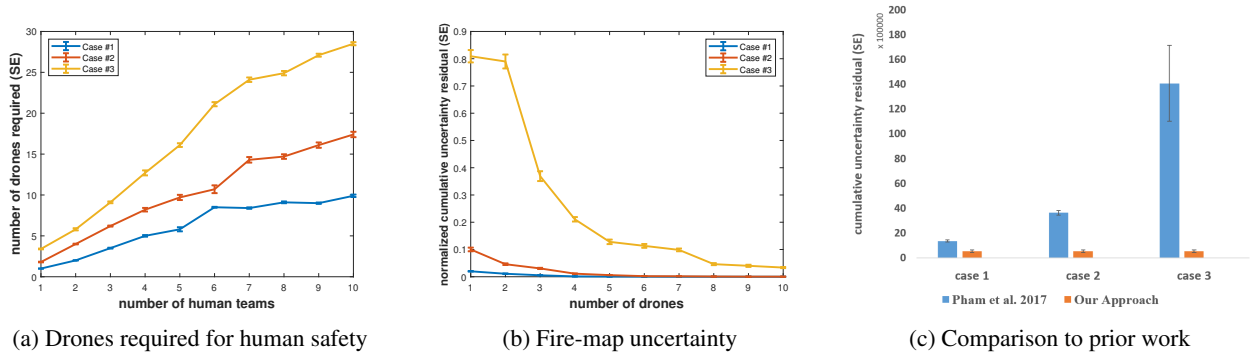
Figure 3: This figure depicts a quantitative evaluation of the human safety analytical bound (Figure 3a), the efficacy of the coverage coordination algorithm (Figure 3b), and a comparison to prior work (Figure 3c)

before recalculating a new path. After T_{UB} has passed, the partitions are revised and an optimal path is recalculated, as fire locations have significantly changed. Once a drone is requested for human safety at firefronts, one of the drones is dismissed and the process is repeated.

4 Empirical Evaluation

4.1 Benchmarks

The first benchmark we compare to is the distributed control framework for dynamic wildfire tracking as proposed by Pham *et al.* [2017]. The distributed control framework includes two controller modules for field coverage and path planning, in which the former is responsible for covering the entire fire, and the latter for path planning. The two controllers are defined as the negative gradients (gradient descent) of objective functions to maximize the area-pixel density of the UAV's fire observations and to maintain safe flight parameters with potential field-based criteria, respectively.

We also compare our approach to a reinforcement learning (RL) baseline. An RL policy network controls a single UAV, and each policy network is identical across UAVs. The network consists of four convolutional layers followed by three fully-connected layers with ReLU activations. A single-channel image with fire locations is the input, and the network outputs a direction for each drone to move. The reward at each step is given as the negative sum of uncertainty over the entire map, encouraging the agent to minimize uncertainty over time. After over 800 episodes, agents continued to exhibit random behavior and failed to find or track any firefronts. While we do not claim that RL cannot work on this application, we believe that our approach is suited to the task, yet failed to produce results. As such, we did not include the RL baseline results in Figure 3c.

4.2 Results

In order to evaluate the efficacy of our proposed human safety module, we performed a comprehensive simulation to determine the number of drones needed to satisfy the uncertainty residual ratio (given in Equation 23) for a range of numbers of humans on a team. We performed the evaluation for all three aforementioned wildfire scenarios for ten trials and calculated the mean and standard error (SE) for each, and the re-

sults of these simulations are in Figure 3a. In our simulations we chose the fire velocity $\dot{q}$ to be 0, 0.5 and 1 for wildfire cases 1, 2, and 3 respectively. We also chose the spawning rate of the fire for case 3 to be at most 3, meaning each fire point can reproduce up to 3 more fire points. As shown in Figure 3a, increasing the number of operating human teams results in a rise in the number of drones required to guarantee the safe conditions. This also holds as the wildfire propagation scenario changes and fire propagates more aggressively.

We also evaluate our distributed coverage platform within a similar framework by calculating the cumulative uncertainty residual while covering the map. The uncertainty residual measure is an indicator of how successful UAVs are in covering all fire points and hotspots, and increases by the number of nodes not covered by any drone. Figure 3b shows the results for the evaluation of our distributed coverage method. For this evaluation, we note that the drones are required to cover the entire fire-map as much as possible, while maintaining an altitude that is both safe and conducive to high-quality imaging. As represented in Figure 3b, for the case of stationary wildfire, drones can easily cover the fire map without missing too many fire points. In case of a fast-growing fire, however, more drones are required to cover the fire-map efficiently and reduce its associated entropy.

Figure 3c shows a comparison between the cumulative uncertainty residual for a team of UAVs controlled by our method and a team a UAVs controlled using the coverage and tracking controller framework presented by Pham *et al.* [2017]. For cases 1, 2, and 3, our approach is able to achieve significantly lower cumulative uncertainty.

5 Conclusion

We have introduced a novel analytical bound on fire propagation uncertainty, allowing for high-quality path planning for real-time wildfire monitoring and tracking while also providing a probabalistic guarantee on humans' safety. Our approach outperforms prior work for distributed control of UAVs for wildfire tracking, as well as a reinforcement learning baseline. In future work, we aim to relax the simplifying assumptions of the FARSITE model and to further explore learning-based techniques.

Appendix

Deriving the Upper-bound time for Wildfire Case 3 (e.g. $T_{UB}^{(C3)}$)

To arrive at this bound, consider Figure 4 as the case detailed in Section 3.1. According to Figure 4, for a specific fire, q the time-varying width and height (e.g. planar length) of the enlarging fire area along X and Y axes can be estimated as in Equations 28 and 29 at the α confidence level, as fires are now allowed to spread for $T_{UB}^{(C3)}$ units of time

$$w(t) \leq 2 \left. \widehat{q_t^x} \right|_\alpha T_{UB}^{(C3)} \tag{28}$$

$$h(t) \leq 2 \left. \widehat{q_t^y} \right|_\alpha T_{UB}^{(C3)} \tag{29}$$

Assuming a vertical scanning pattern as shown, we round up the maximum possible $w(t)$ and thus the total number of passes the drone would take from left to right is given by,

$$n(t) \leq \left\lceil \frac{2 \left. \widehat{q_t^x} \right|_\alpha T_{UB}^{(C3)}}{g} \right\rceil \tag{30}$$

and the total distance traversed for each pass is

$$d(t) = 2 \left. \widehat{q_t^y} \right|_\alpha T_{UB}^{(C3)} \tag{31}$$

and finally the total pass traversed is

$$d^{tot}(t) = n(t)h(t) \tag{32}$$

Accordingly the time required for one firefront point to escape the FOV of a specific drone d with velocity v can be calculated as

$$\tau_q(t) = \frac{d^{tot}(t)}{v} \tag{33}$$

$$= \frac{n(t)h(t)}{v} \tag{34}$$

$$= \frac{\left\lceil \frac{2 \widehat{q_t^x}\big|_\alpha T_{UB}^{(C3)}}{g} \right\rceil 2 \left. \widehat{q_t^y} \right|_\alpha T_{UB}^{(C3)}}{v} \tag{35}$$

Now, the time required for all of the fire-points will be the summation over all τ_q in Equation 35; however we must note that each center fire point spreading also moves and the upper bound time derived for case 2 in Equation 18 (e.g. $T_{UB}^{(C2)}$) have to be added to this summation. Therefore, the upper bound time for case 3 can be estimated as in Equation 36

$$T_{UB}^{(C3)} = \left. T_{UB}^{(C2)} \right|_{C3} + \sum_q \frac{2}{v} \left. \widehat{q_t^y} \right|_\alpha T_{UB} \left\lceil \frac{2 \left. \widehat{q_t^x} \right|_\alpha T_{UB}^{(C3)}}{g} \right\rceil \tag{36}$$

We need to solve Equation 36 for $T_{UB}^{(C3)}$ to find the final equation to obtain the upper bound. For this purpose, we make the following two simplifying assumptions: First, we remove the ceiling operator and add one to the term inside the operator to achieve continuity. , as shown in Equation 37.

$$\left\lceil \frac{2 \left. \widehat{q_t^x} \right|_\alpha T_{UB}^{(C3)}}{g} \right\rceil \leq \frac{2 \left. \widehat{q_t^x} \right|_\alpha T_{UB}^{(C3)}}{g} + 1 \tag{37}$$
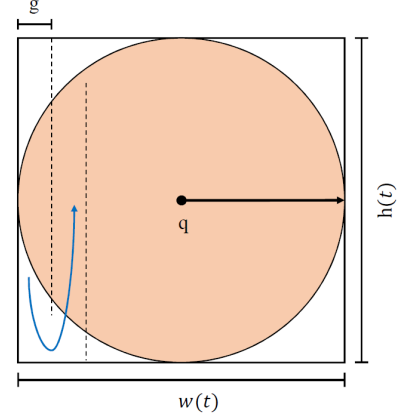

Figure 4: The third wildfire scenario where fire can move and spawn quickly. The large red circle shows the potential area engulfed by the growth of each firefront. Parameter g represents the width of the UAV's FOV. The blue arrow represents UAV's partial trajectory while monitoring the fire (vertical scanning pattern is assumed)

Second, we adopt a similar approach to Case 2 by assuming the area required to cover to account for the growth of each fire location is upper-bounded by $|Q|$ times the area of growth for a hypothetical fire growing quickest. (Equation 38).

$$\sum_q \left. \widehat{q_t^y} \right|_\alpha T_{UB} \left\lceil \frac{2 \left. \widehat{q_t^x} \right|_\alpha T_{UB}^{(C3)}}{g} \right\rceil \leq |Q|\zeta^\alpha \left\lceil \frac{2\zeta^\alpha T_{UB}^{(C3)}}{g} \right\rceil \tag{38}$$

With these two conservative, simplifying assumptions, the bound in Equation 36 can be revised as below

$$T_{UB}^{(C3)} = \left. T_{UB}^{(C2)} \right|_{C3} + \frac{2|Q|\zeta^\alpha T_{UB}^{(C3)}}{v} \left[\frac{2\zeta^\alpha T_{UB}^{(C3)}}{g} + 1 \right] \tag{39}$$

$$T_{UB}^{(C3)} - \frac{2|Q|\zeta^\alpha T_{UB}^{(C3)}}{v} \left[\frac{2\zeta^\alpha T_{UB}^{(C3)}}{g} + 1 \right] = \left. T_{UB}^{(C2)} \right|_{C3} \tag{40}$$

$$T_{UB}^{(C3)} - \frac{2|Q|\zeta^\alpha T_{UB}^{(C3)}}{v} \left[\frac{2\zeta^\alpha T_{UB}^{(C3)}}{g} + 1 \right] = \frac{MST}{\frac{v}{2} - 2\zeta^\alpha(|Q| - 1)} \tag{41}$$

Note that Equation 41 is in the form of $z - az(bz + 1) = \delta$ general quadratic equations with $z = T_{UB}^{(C3)}$, which can be simplified to $\gamma z^2 - \beta z + \delta = 0$, where $\gamma = ab$ and $\beta = 1 + a$ and they can be calculated as below

$$\gamma = \frac{4|Q|(\zeta^\alpha)^2}{gv} \tag{42}$$

$$\beta = 1 + \frac{2|Q|\zeta^\alpha}{v} \tag{43}$$

$$\delta = \frac{MST}{\frac{v}{2} - 2\zeta^\alpha(|Q| - 1)} \tag{44}$$

and eventually, from the solution to general quadratic equations we know that the upper-bound traversal time $T_{UB}^{(C3)}$ allowed to maintain the track quality of each fire for case 3 can be obtained as in Equation 45

$$T_{UB}^{(C3)} = \frac{-\beta + \sqrt{\beta^2 - 4\gamma\delta}}{2\gamma} \tag{45}$$

Calculating the Jacobian Matrices and the Gradients

To calculate we first reform the state transition equation in 24 to account for all aforementioned associating parameters as below

$$\left[\mathcal{S}_t\right]_{8\times 1} = \left[\left.\frac{\partial f}{\partial \mathcal{S}_i}\right|_{\hat{\mathcal{S}}_{t-1|t-1}}\right]_{8\times 8}\left[\mathcal{S}_{t-1}\right]_{8\times 1} + \omega_t \quad (46)$$

where The process noise ω_t should account for both stochasticity in fire behavior and propagation model inaccuracy and is modeled by a zero mean white Gaussian noise. Accordingly, we form the state transition Jacobian matrices F_t in Equation 7 including partial derivatives of wildfire propagation dynamics in Equations 1 and 2 with respect to all of the variables in state vector $\mathcal{S}_t$. Note that the parameters R_t, U_t and U_t are not necessarily dynamic with time and it is fairly reasonable to consider this physical parameters as constants for short periods of time. However, in case of analyzing the system for longer durations, temporal dynamics may apply (Delamatar *et al.* [2013]) specifically due to changes in windspeed and velocity. Exact estimation of temporal dynamics related to these parameters are out of the scope of the current study since we assume locality in time and space according to FARSITE (Finney [1998]). The resulting Jacobian matrix will take the form as in Equation 26. To calculate the partial derivatives in Equation 26 we need the fire dynamics through wildfire mathematical model. By ignoring the superscript i in Equations 1 and 2, without losing generality, $\dot{q}_t$ can be estimated for each propagating firefront by Equations 47-49, where $\dot{q}_t^x$ and $\dot{q}_t^x$ are firefront first-order dynamic for *X* and *Y* coordinates, and a, b, c, d and l are constants

$$\dot{q}_t^x = C(R_t, U_t)\sin(\theta_t) \quad (47)$$
$$\dot{q}_t^y = C(R_t, U_t)\cos(\theta_t) \quad (48)$$

where

$$C(R_t, U_t) = R_t\left(1 - \frac{LB(U_t)}{LB(U_t) + \sqrt{GB(U_t)}}\right) \quad (49)$$

and

$$LB(U_t) = ae^{bU_t} + ce^{-dU_t} + l \quad (50)$$
$$GB(U_t) = LB(U_t)^2 - 1 \quad (51)$$

Now, the derivatives of q_t^x and q_t^y with respect to the parameters R_{t-1}, U_{t-1} and θ_{t-1} are computed by applying the chain-rule and using Equation 47-51 as follows, where $\mathcal{D}(\theta)$ equals $\sin\theta$ and $\cos\theta$ for X and Y axis respectively.

$$\frac{\partial q_t}{\partial \theta_{t-1}} = C(R_t, U_t)\frac{\partial \mathcal{D}(\theta)}{\partial \theta}\delta t \quad (52)$$

$$\frac{\partial q_t}{\partial R_{t-1}} = \left(1 - \frac{LB(U_t)}{LB(U_t) + \sqrt{GB(U_t)}}\right)\mathcal{D}(\theta)\delta t \quad (53)$$

$$\frac{\partial q_t}{\partial U_{t-1}} = \frac{R_{t'}\left(LB(U_{t'})\frac{\partial GB(U_{t'})}{\partial U_{t'}} - GB(U_{t'})\frac{\partial LB(U_{t'})}{\partial U_{t'}}\right)}{\left(LB(U_{t'}) + \sqrt{GB(U_{t'})}\right)^2}\mathcal{D}(\theta)\delta t$$
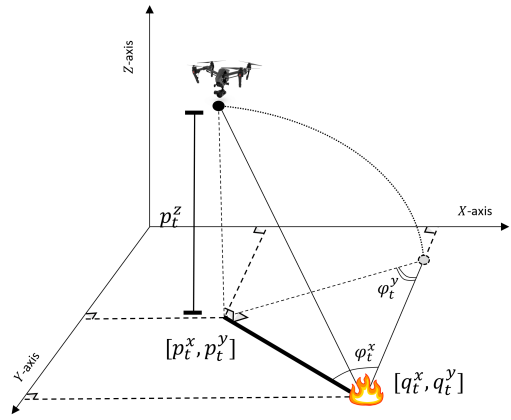$$(54)$$

Figure 5: The UAV observation model.

To calculate the observation Jacobian matrix H_t in Equation 27 and its gradients, we first consider Figure 5 which depicts the observation model through which UAVs perceive the fire.

Accordingly, the observation mapping equation in 25 will be now presented as

$$\left[\hat{\Phi}_t\right]_{5\times 1} = \left[\left.\frac{\partial h}{\partial \Phi_i}\right|_{\Phi_{t|t}}\right]_{5\times 8}\left[\Phi_t\right]_{8\times 1} + \nu_t \quad (55)$$

The angle-parameters (i.e. φ_t^x and φ_t^y) contains information regarding both firefront location $[q_t^x, q_t^y]$ and UAV coordinates $[p_t^x, p_t^y]$. Considering $p_t^d = [p_t^x, p_t^y, p_t^z]^T$ as the desired current UAV pose, there will be errors associated with all of these coordinates. This will affect UAVs ability to extrapolate where the fire is on the ground and is very important to be taken into account. The observation noise is modeled as a zero-mean white Gaussian noise. Note that errors in X, Y and Z axes coordinates of a drone are loosely correlated and thus, we also incorporate non-diagonal elements in observation noise covariance matrix R_t. According to Figure 5, by projecting the looking vector of UAV to planar coordinates, the angle parameters are calculated as below

$$\varphi_t^x = \tan^{-1}\left(\frac{q_t^x - p_t^x}{p_t^z}\right) \quad (56)$$

$$\varphi_t^y = \tan^{-1}\left(\frac{q_t^y - p_t^y}{p_t^z}\right) \quad (57)$$

. The observation Jacobian matrix H_t is presented in Equation 27 where the partial derivatives are derived using Equations 56 and 57 as follows

$$\frac{\partial \varphi_t^x}{\partial q_t^x} = \frac{1}{1 + \left(\frac{q_t^x - p_t^x}{p_t^z}\right)^2}\left(\frac{1}{p_t^z}\right) \quad (58)$$

$$\frac{\partial \varphi_t^x}{\partial p_t^x} = \frac{1}{1 + \left(\frac{q_t^x - p_t^x}{p_t^z}\right)^2}\left(\frac{-1}{p_t^z}\right) \quad (59)$$

$$\frac{\partial \varphi_t^x}{\partial p_t^z} = \frac{1}{1 + \left(\frac{q_t^x - p_t^x}{p_t^z}\right)^2}(q_t^x - p_t^z)\left(\frac{-1}{(p_t^z)^2}\right) \quad (60)$$

similar Equations as above holds for *Y*-axis with q_t^y and p_t^y.

References

Shahrokh Akhlaghi, Ning Zhou, and Zhenyu Huang. Adaptive adjustment of noise covariance in kalman filter for dynamic state estimation. In *2017 IEEE Power & Energy Society General Meeting*, pages 1–5. IEEE, 2017.

Randal Beard, Derek Kingston, Timothy W McLain, and Derek Nelson. Decentralized cooperative aerial surveillance using fixed-wing miniature uavs. 2006.

David W Casbeer, Derek B Kingston, Randal W Beard, and Timothy W McLain. Cooperative forest fire surveillance using a team of small unmanned air vehicles. *International Journal of Systems Science*, 37(6):351–360, 2006.

Doo-Hyun Cho and Han-Lim Choi. A traveling salesman problem-based approach to observation scheduling for satellite constellation. *International Journal of Aeronautical and Space Sciences*, pages 1–8, 2019.

Han-Lim Choi, Luc Brunet, and Jonathan P How. Consensus-based decentralized auctions for robust task allocation. *IEEE transactions on robotics*, 25(4):912–926, 2009.

PL Delamatar, AQ Finley, and Chad Babcock. Downloading and processing noaa hourly weather station data. *dim (st)*, 1(30538):12, 2013.

Mark A Finney. Farsite: Fire area simulator-model development and evaluation. *Res. Pap. RMRS-RP-4, Revised 2004. Ogden, UT: US Department of Agriculture, Forest Service, Rocky Mountain Research Station. 47 p.*, 4, 1998.

Kazuhiko Fujiwara and Jun-ichi Kudoh. Forest fire detection in 2001 using three-dimensional histogram. In *Geoscience and Remote Sensing Symposium, 2002. IGARSS'02. 2002 IEEE International*, volume 4, pages 2057–2059. IEEE, 2002.

Bruce Golden, Lawrence Bodin, T Doyle, and W Stewart Jr. Approximate traveling salesman algorithms. *Operations research*, 28(3-part-ii):694–711, 1980.

Insurance Information Institute. Facts + statistics: Wildfires, 2018.

Rudolph E Kalman and Richard S Bucy. New results in linear filtering and prediction theory. *Journal of basic engineering*, 83(1):95–108, 1961.

Rudolf Emil Kalman et al. Contributions to the theory of optimal control. *Bol. Soc. Mat. Mexicana*, 5(2):102–119, 1960.

Rudolph Emil Kalman. A new approach to linear filtering and prediction problems. *Journal of basic Engineering*, 82(1):35–45, 1960.

J-I Kudoh and Kazuma Hosoi. Two dimensional forest fire detection method by using noaa avhrr images. In *Geoscience and Remote Sensing Symposium, 2003. IGARSS'03. Proceedings. 2003 IEEE International*, volume 4, pages 2494–2495. IEEE, 2003.

Manish Kumar, Kelly Cohen, and Baisravan Homchaudhuri. Cooperative control of multiple uninhabited aerial vehicles for monitoring and fighting wildfires. *Journal of Aerospace Computing, Information, and Communication*, 8(1):1–16, 2011.

Gilbert Laporte. The vehicle routing problem: An overview of exact and approximate algorithms. *European journal of operational research*, 59(3):345–358, 1992.

José Ramiro Martinez-de Dios, Begoña C Arrue, Aníbal Ollero, Luis Merino, and Francisco Gómez-Rodríguez. Computer vision techniques for forest fire perception. *Image and vision computing*, 26(4):550–562, 2008.

Mitchell McIntire, Ernesto Nunes, and Maria Gini. Iterated multi-robot auctions for precedence-constrained task scheduling. In *Proceedings of the 2016 International Conference on Autonomous Agents & Multiagent Systems*, pages 1078–1086. International Foundation for Autonomous Agents and Multiagent Systems, 2016.

Luis Merino, Fernando Caballero, J Ramiro Martinez de Dios, Ivan Maza, and Aníbal Ollero. Automatic forest fire monitoring and measurement using unmanned aerial vehicles. In *Proceedings of the 6th International Congress on Forest Fire Research. Edited by DX Viegas. Coimbra, Portugal*. Citeseer, 2010.

Ernesto Nunes and Maria Gini. Multi-robot auctions for allocation of tasks with temporal constraints. In *Twenty-Ninth AAAI Conference on Artificial Intelligence*, 2015.

Elsa Pastor, Luis Zárate, Eulalia Planas, and Josep Arnaldos. Mathematical models and calculation systems for the study of wildland fire behaviour. *Progress in Energy and Combustion Science*, 29(2):139–153, 2003.

Huy X Pham, Hung M La, David Feil-Seifer, and Matthew Deans. A distributed control framework for a team of unmanned aerial vehicles for dynamic wildfire tracking. In *Intelligent Robots and Systems (IROS), 2017 IEEE/RSJ International Conference on*, pages 6648–6653. IEEE, 2017.

Murali R Rajamani. *Data-based techniques to improve state estimation in model predictive control*. PhD thesis, Citeseer, 2007.

Mac Schwager, Brian J Julian, Michael Angermann, and Daniela Rus. Eyes in the sky: Decentralized control for the deployment of robotic camera networks. 2011.

Darko Stipaniev, Maja tula, Ljiljana Krstini, Damir and, Toni Jakov, and Bugari. Advanced automatic wildfire surveillance and monitoring network. In *6th International Conference on Forest Fire Research, Coimbra, Portugal.(Ed. D. Viegas)*, 2010.

PB Sujit, Derek Kingston, and Randy Beard. Cooperative forest fire monitoring using multiple uavs. In *Decision and Control, 2007 46th IEEE Conference on*, pages 4875–4880. IEEE, 2007.

Michele Taragna. Kalman filter theory. Technical report, Dipartimento di Automatica e Informatica Politecnico di Torino, 2011.

Paolo Toth and Daniele Vigo. *The vehicle routing problem*. SIAM, 2002.

Xingyin Wang, Bruce Golden, and Edward Wasil. A steiner zone variable neighborhood search heuristic for the close-enough traveling salesman problem. *Computers & Operations Research*, 101:200–219, 2019.

Chi Yuan, Youmin Zhang, and Zhixiang Liu. A survey on technologies for automatic forest fire monitoring, detection, and fighting using unmanned aerial vehicles and remote sensing techniques. *Canadian journal of forest research*, 45(7):783–792, 2015.